STRUCTURAL DYNAMICS MODELING AND MACHINE LEARNING FOR INTEGRAL BLADE ROTOR MILLING

Gregory M. Corson[1], Jaydeep Karandikar[2], Tony Schmitz[1,2]
[1]Mechanical, Aerospace, and Biomedical Engineering
University of Tennessee, Knoxville
Knoxville, TN 37996, USA
[2]Manufacturing Science Division
Oak Ridge National Laboratory
Oak Ridge, TN 37830, USA

INTRODUCTION

In this paper, a Bayesian machine learning framework is developed to model the process dynamics and optimize the milling parameters for an integral blade rotor (IBR), or blisk. The IBR was selected as a use case due to the challenges in machining dynamically compliant designs from wrought or forged stock made from difficult-to-machine materials. Parameter selection requires a model-based approach because: 1) the structural dynamics depend on the tool-holder-spindle and workpiece; and 2) the structural dynamics dictate combinations of spindle speed and depth of cut that result in chatter, a self-excited vibration that causes large cutting forces, poor surface finish, and rapid tool wear. While conservative combinations may be selected, these non-optimal parameters increase cycle time, cost, and energy use.

Typically, machinists and computer numerically controlled (CNC) toolpath programmers rely on prior experience and information provided in machining handbooks or from the tool manufacturer for parameter selection. However, because these parameters are established without knowledge of the selected dynamic system, they may be sub-optimal or unachievable (i.e., produce chatter) [1]. The case study presented here uses a combination of physics-based models, machine learning, and in-process data to provide physics-informed Bayesian machine learning (PIBML) that improves the accuracy of model predictions over traditional machine learning or physics-based methods individually.

MODELING

Bayesian machine learning

Bayesian machine learning (BML) defines a probabilistic model of the milling stability map given test results (stable or unstable) over a spindle speed-axial depth of cut domain. Equation 1 shows Bayes' rule for updating the probability of stability at a selected spindle speed-axial depth combination using the stability result from a test point [2].

$$p(s_g|r_t) = \frac{p(r_t|s_g)p(s_g)}{p(r_t)} \quad (1)$$

In Eq. 1, *p* denotes probability, *s* denotes stability, *r* denotes the test result, subscript *g* and *t* denote a selected and test point combination of spindle speed and axial depth. From Bayes' rule, the posterior probability of stability at *g* given the test result at *t* is the product of the prior probability of stability at *g*, and the likelihood probability of the experimental result given *g* is stable, divided by the marginal probability of the result.

Figure 1 illustrates the BML approach [2], where the top plot displays the prior, which assumes the probability of stability (1) decreases with axial depth (darker regions are stable, lighter regions are unstable). The prior is then updated with experimental data as test cuts are labeled stable or unstable according to frequency content of the milling sound. A microphone in the machining enclosure captures the sound of the milling operation. Frequency content outside the tooth passing frequency and its multiples or harmonics indicates chatter [3]. With the new information, the prior is tuned using Bayes' rule (Eq. 1) [2].

Figure 1 displays the posterior (or tuned) probability of stability given stable (middle) and unstable/chatter (bottom) experimental results. A test selection strategy is implemented to find the optimal parameters with the highest material removal rate, where the expected improvement is maximized for each experiment [2].

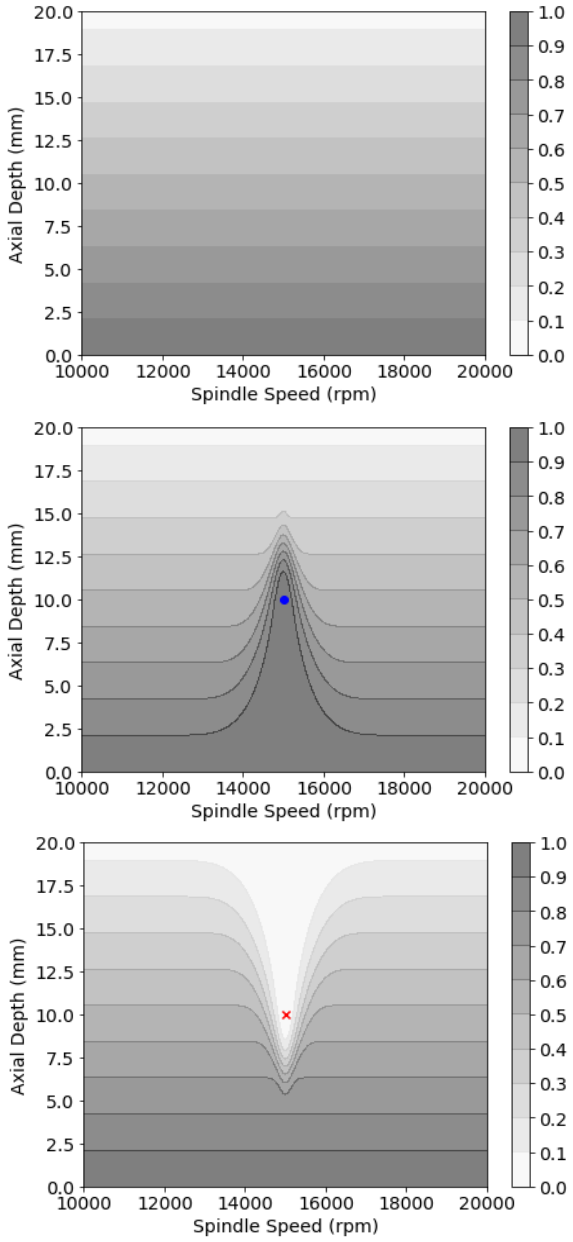

FIGURE 1: (Top) prior distribution of milling stability. (Middle) posterior probability of stability for a stable test. (Bottom) posterior probability of stability for an unstable test.

The BML prior in this work uses a frequency-domain milling stability solution that requires two major inputs. First, a model that relates the milling parameters to resultant cutting force. Second, the tool tip frequency response function (FRF) that describes the vibratory response of the tool-holder-machine-spindle assembly in use.

Finite element force modeling

A GOM ATOS-Q structured light scanner was used to measure the edge geometry of the selected endmills. These measurements were inputs to Third Wave Systems AdvantEdge software, a commercially-available, finite element package tailored to predict cutting forces. Orthogonal cutting simulations were performed for a fixed chip width, *b*, and variable chip thickness, *h*. The software's material models for 304 stainless steel (SST) and 6Al-4V titanium (Ti) were used to calculate the cutting force components in the tangential (*t*) and normal (*n*) directions. The mean force was plotted as a function of chip thickness and a linear regression was used to identify the slope and intercept values [3]. These values provided the mechanistic force model coefficients in Eqs. 2 and 3, where the slopes provided the cutting coefficients (*c* subscripts) and the intercepts provided the edge coefficients (*e* subscripts). The coefficient values are listed in Table 1.

$$F_t = k_{tc} bh + k_{te} b \quad (2)$$

$$F_n = k_{nc} bh + k_{ne} b \quad (3)$$

TABLE 1: Cutting coefficients for mechanistic force models.

	Coefficients			
Material	k_{tc} (N/mm^2)	k_{nc} (N/mm^2)	k_{te} (N/mm)	k_{ne} (N/mm)
304 SST	1618	792	138	76
6Al-4V Ti	1839	662	235	81

Receptance coupling substructure analysis

Receptance coupling substructure analysis (RCSA) is applied here to predict the tool tip receptance, or FRF, rather than performing a tap test to measure the FRF [1]. In the RCSA approach, a simple geometry artifact is first clamped in the spindle and measured by tap testing, where an instrumented hammer is used to excite the assembly and a low-mass

accelerometer is used to measure the vibration response. Second, the spindle-machine FRF is calculated by decoupling the artifact in simulation (i.e., inverse RCSA). Third, the tool and holder models are coupled to the spindle-machine FRF to predict the tool tip FRF [5-6]; see Fig. 2.

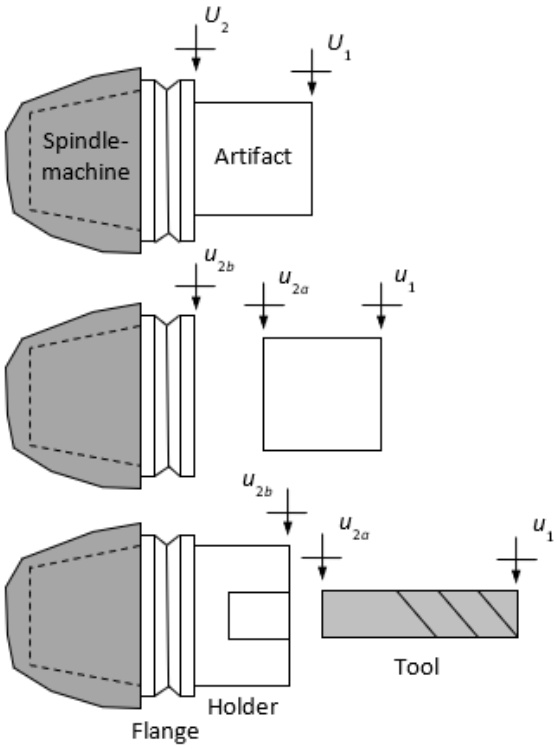

FIGURE 2: RCSA model. (Top) an artifact is clamped in the spindle and measured. (Middle) the spindle-machine FRF is calculated by inverse RCSA. (Bottom) the tool and holder models are coupled to the spindle-machine FRF to predict the tool tip FRF.

In RCSA, Eq. 4 is applied to determine the spindle-machine FRFs, where the frequency-dependent R_{ij} (component, lower case coordinates) and G_{ij} (assembly, upper case coordinates) FRF matrices are defined in Eq. 5. In Eq. 5, *x*/*X* is lateral displacement, *f*/*F* is a harmonic force, θ/Θ is rotation, and *m*/*M* is a harmonic moment (or couple). The tool tip FRF is predicted using Eq. 6, where the R_{11}, R_{12a}, R_{2a2a}, and R_{2a1} matrices are defined by the free-free boundary condition tool FRFs, R_{2b2b} represents a rigid connection of the spindle-machine and holder, the (1,1) location in the G_{11} matrix contains the required FRF for stability modeling, and the connection matrix, *K*, between the holder and tool is shown in Eq. 7, where *k* and *c* are stiffness and viscous damping and ω is the frequency. Uncertainty exists for *k* and *c* which gives uncertainty in the predicted tool tip FRF. Uncertainty also exists in the cutting force model. These uncertainties are used to calculate the initial probabilistic stability boundary (prior).

$$R_{2b2b} = R_{2a1}(R_{11} - G_{11})^{-1}R_{12a} - R_{2a2a} \quad (4)$$

$$R_{ij} = \begin{bmatrix} \frac{x_i}{f_j} & \frac{x_i}{m_j} \\ \frac{\theta_i}{f_j} & \frac{\theta_i}{m_j} \end{bmatrix}, G_{ij} = \begin{bmatrix} \frac{X_i}{F_j} & \frac{X}{M_j} \\ \frac{\Theta_i}{F_j} & \frac{\Theta_i}{M_j} \end{bmatrix} \quad (5)$$

$$G_{11} = R_{11} - R_{12a}\left(R_{2a2a} + R_{2b2b} + \frac{1}{K}\right)^{-1} R_{2a1} \quad (6)$$

$$K = \begin{bmatrix} 0 & k + i\omega c \\ k + i\omega c & 0 \end{bmatrix} \quad (7)$$

Physics-informed Bayesian machine learning

A physics-informed prior was generated by propagating uncertainties in the stability model inputs (k_{tc} and k_{nc} from Eqs. 2 and 3, *k* and *c* from Eq. 7) to uncertainty in the stability limit using a Monte Carlo simulation. In each iteration, a random sample was selected from the {k_{tc}, k_{nc}, *k*, *c*} normal distributions. For k_{tc} and k_{nc}, the standard deviations were 25% of the mean values from Table 1. For *k* and *c*, the mean values were 6×10^6 N/rad and 26 N-s/rad (based on prior modeling efforts for ER32 collet holders). The standard deviations were again 25% of the mean values. The stability limit was then calculated using these inputs. Figure 3 displays the variation in tool tip FRFs in the *x* (feed) and *y* directions and Fig. 4 shows the corresponding distribution in stability limits for slotting in 304 stainless steel.

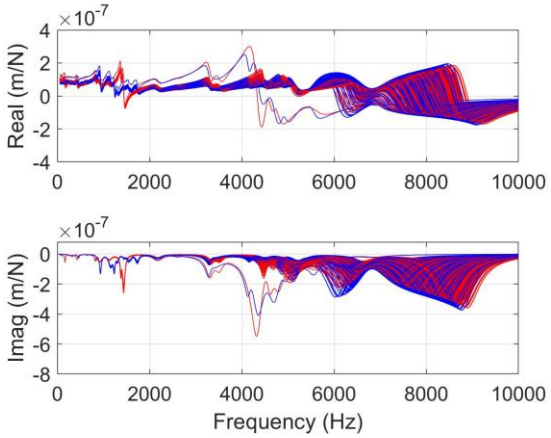

FIGURE 3. Tool tip FRFs predicted by RCSA for the x (red) and y (blue) directions

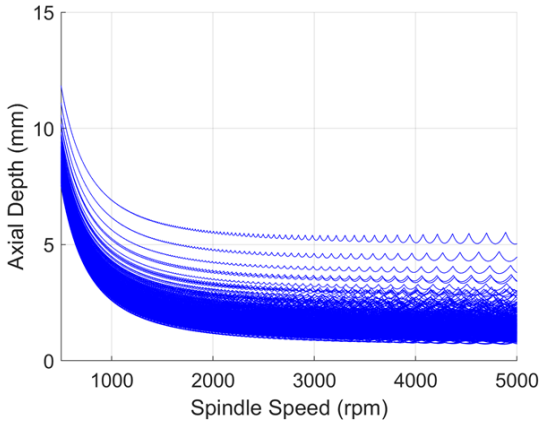

Figure 4: Stability limits calculated using the uncertain FRFs and force model coefficients.

The spindle speed-axial depth of cut domain was discretized and the prior probability of stability was determined by calculating the ratio of stability boundaries where the respective point was stable versus unstable at the same spindle speed. The prior probability of stability was used in the PIBML approach to calculate the posterior probability of stability after new information was obtained from test results.

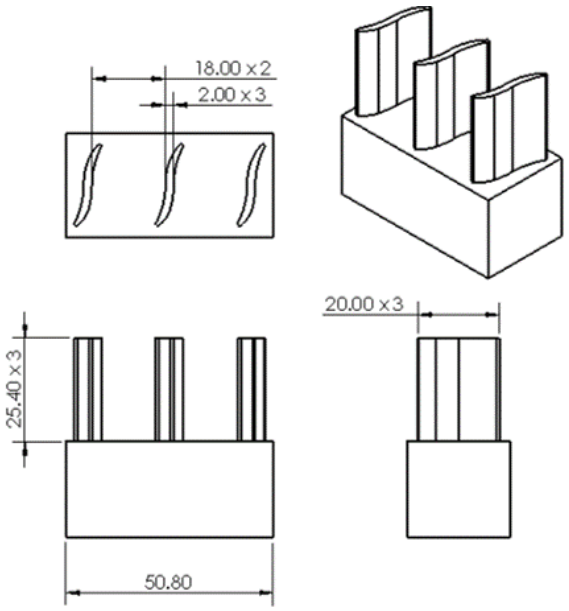

FIGURE 5. IBR geometry (dimensions in mm).

RESULTS

304 stainless steel IBR

The IBR geometry displayed in Fig. 5 was selected and machined using a 12.7 mm diameter endmill with four teeth and 0.38 mm corner radii. The manufacturer recommended an axial depth of 6.35 mm and spindle speed range of 2215 rpm to 2674 rpm for slotting. The IBRs were machined from pieces of wrought stock material, so a slotting condition (100% radial engagement) was required to remove the material between the blades. Since the stability limit is lowest for slotting conditions, this operation was the limitng factor that dictated the maximum axial depth for each layer (the blades were rough and finish machined one axial layer at a time from tip to root).

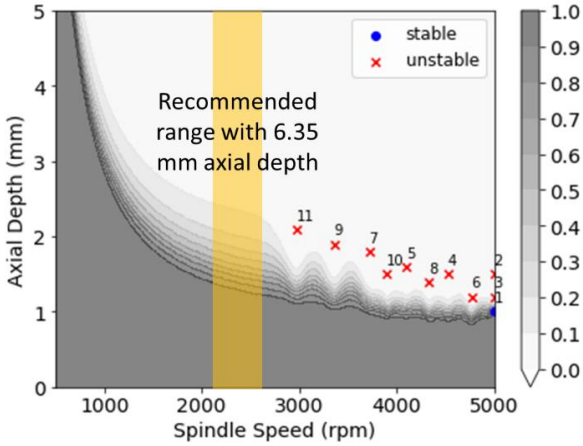

FIGURE 6: 304 stainless steel results.

As shown in Fig. 6, the tool manufacturer's recommended axial depth was predicted to be unstable for all spindle speeds according to the prior so tests was performed to identify optimal machining parameters. The PIBML model only needed 11 test cuts to converge to the optimal combination of spindle speed (5000 rpm) and axial depth (1.0 mm). The spindle speed was limited to 5000 rpm to provide adequate tool life for machining the entire IBR with a single endmill. These parameters were then input to a computer-aided manufacturing (CAM) software (Fusion 360) for toolpath programming.

Production Module™, a commercially-available federate scheduling software from Thid Wave Systems, was used to optimize the program and decrease cycle time. Production Module™ provided a 15% cycle time reduction relative to the original CAM tool path. The posterior, test points, and machining results are shown in Fig. 6.

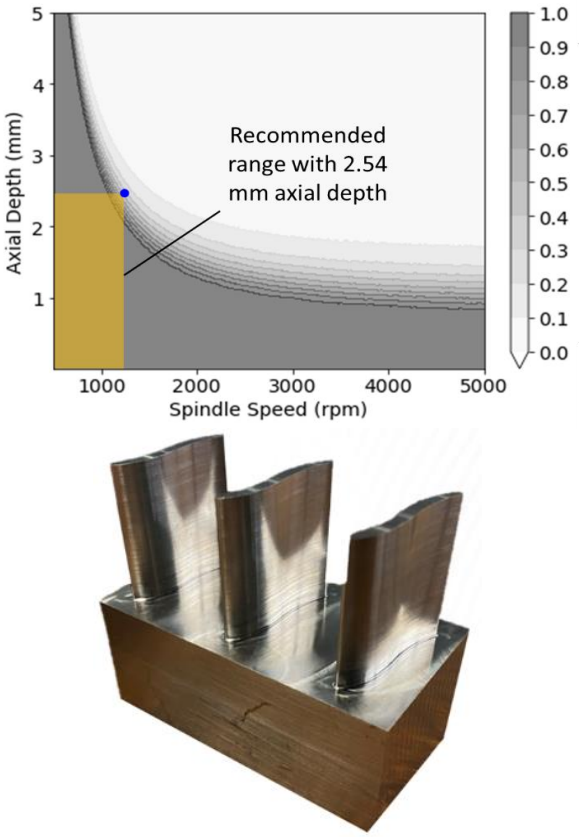

FIGURE 7: 6Al-4V titanium results.

6Al-4V titanium IBR

The 12.7 mm diameter endmill with four teeth and 0.38 mm corner radii was also selected for machining the 6Al-4V titanium IBR. The tool manufacturer recommended a spindle speed range from 398 rpm to 1314 rpm and axial depth of 2.54 mm for slotting in 6Al-4V titanium. The most productive condition (highest rate of material removal) for this range, i.e., 1314 rpm spindle speed and 2.54 mm axial depth, had a 50% probability of stability according to the physics-informed prior. A cutting test validated that these parameters produced stable cutting conditions. Therefore, no further testing was required and the IBR tool path was programmed using the 1314 rpm-2.54 mm parameters. Production Module™ optimization provided a 7% cycle time reduction. The prior and machined IBR are displayed in Fig. 7.

CONCLUSIONS

A physics-informed Bayesian machine learning (PIBML) method was described that used two physics-based models: 1) a prediction of the tool tip dynamics via RCSA; and 2) a mechanistic force model provided by orthogonal, finite element cutting simulations. The uncertainty of these model inputs were propagated into the output predicted milling stability by a Monte Carlo simulation. These uncertain stability limits were used to generate a probabilistic stability map that represented knowledge about the milling stability of the selected tool-holder-machine assembly and workpiece material before cuts were performed, referred to as the prior.

For the 304 stainless steel workpiece material case, the recommended axial depth of cut was unstable over the full spindle speed range. The prior was then updated through experimental testing where cuts were declared stable or unstable according to the sound frequency content. Machining parameters were then selected based on the posterior probability of stability. The toolpaths were further optimized by a feedrate scheduling software and were then used to machine non-proprietary IBRs.

For the 6Al-4V titanium workpiece material, the highest material removal rate condition within the recommended axial depth and spindle speed range was predicted to be stable with a 50% probability. Machining trials confirmed stable machining performance. The feedrates of the toolpaths with the recommended parameters were optimized and IBRs were machined. The disagreement between manufacturer recommendations and optimized performance for the 304 SST milling case emphasizes the need for broad implementation of PIBML approaches, as demonstrated here, to increase machining productivity and efficiency.

ACKNOWLEDGEMENTS

This research was supported by MxD project number 20-11-04 Physics-Guided Machine Learning (PGML) for CNC Milling. This material is based on research sponsored by Office of the Under Secretary of Defense for Research and Engineering, Strategic Technology Protection and Exploitation, Defense Manufacturing Science and Technology Program under agreement number W15QKN-19-3-0003 between MxD and

the Government. The U.S. Government is authorized to reproduce and distribute reprints for Governmental purposes.

REFERENCES

[1] Corson G, Karandikar J, Schmitz T. Integral blade rotor milling improvement by physics-guided machine learning. ASPE 36th Annual Meet 2021.

[2] Schmitz TL, Donaldson RR. Predicting High-Speed Machining Dynamics by Substructure Analysis. CIRP Ann 2000;49:303–8.

[3] Schmitz TL, Davies MA, Kennedy MD. Tool Point Frequency Response Prediction for High-Speed Machining by RCSA. J Manuf Sci Eng 2001;123:700–7.

[4] Altintaş Y, Budak E. Analytical Prediction of Stability Lobes in Milling. CIRP Annals 1995;44(1):357-62.

[5] Karandikar J, Honeycutt A, Schmitz T, Smith S. Stability boundary and optimal operating parameter identification in milling using Bayesian learning. Journal of Manufacturing Processes 2020;56:1252–62.